Numerical investigation of a jet-and-vortex-actuator without and with cross-flow boundary layer

Muhammad Aqeel Rashad, Ulrich Rist *

Institut für Aerodynamik & Gasdynamik, Universität Stuttgart, Pfaffenwaldring 21, 70550 Stuttgart, Germany

ARTICLE INFO

ABSTRACT

In this study we consider an active flow control actuator which was first investigated experimentally by Lachowicz et al. (1999a,b) and called "Jet and Vortex Actuator" (JaVA). The Fluent® CFD software package has been used because of its ability to employ user-defined functions for specification of the unsteady boundary conditions and a sliding mesh interface for discretization of the moving parts of the JaVA. Three cases are presented, one without cross flow and two with a cross-flow boundary layer. The difference in the latter two is that the actuator arrangement with respect to the cross flow is reversed from one case to the other. The results for the first case prove that the available experimental results can be reproduced in a computational study and that the numerical simulation provides additional information because it covers the unsteady details as well. The other two cases show that the actuator increases the wall-normal velocity gradient by a redistribution of momentum within the boundary layer, especially when the wide gap of the actuator is behind the small gap and the moving actuator plate.

© 2011 Elsevier Inc. All rights reserved.

1. Introduction and background

Actuator flow control can be of two kinds: passive and active, cf. Gad-el-Hak and Bushnell (1991). For improving aircraft aerodynamic performance existing flow control has been mostly passive, Gad-el-Hak (2000). Passive control means that fixed devices are used to control the flow. Typical examples are fixed vortex generators used on high-lift systems, cf. Lin (2002). At landing/takeoff conditions, the vortex generators transport high-momentum fluid from the outer boundary layer towards the wing surface, energizing the near-wall layer to prevent separation. Although these devices are simple and low cost in manufacturing, they have two significant disadvantages: First, passive flow control devices cannot be optimized for multiple flight conditions (landing, take-off, maneuver) and second, they add extra drag in conditions where they are no longer needed. Active control can defeat these disadvantages and optimize overall performance of the system, cf. Gad-el-Hak (2001). According actuators can be used in multiple flight conditions in contrast to passive flow control devices. Furthermore, an active flow-control actuator produces negligible drag when the system is not actuated. Future aircraft will need active-flow control devices to meet increasing demands on efficiency and lower emissions (noise and fuel burnt), cf. Zhong et al. (2007) and Tang et al. (2007). Corresponding devices typically use suction and blowing in a more or less cyclic manner. These devices may be installed within the external surfaces of the airframe for separation control, noise reduction and control of laminar-turbulent transition or inside the engines and other tubing to increase their efficiency or to make them quieter. A great variety of possible actuator designs are proposed and studied by many researchers and there is a lot of activity which is not free of problems, e.g. Glezer and Amitay (2002), Lockerby and Carpenter (2004) and Godard et al. (2006). Foreseeable open problems are the durability and resistance of these actuators with respect to dirt and use, maximizing their efficiency and keeping their weight and manufacturing costs reasonably low. There is a clear need to study and understand the influence of the different geometrical parameters on the flow induced by an actuator and also to accurately predict its behavior. Therefore, in the present study an actuator which was originally presented by Lachowicz et al. (1999a) is used as a reference to contribute to this research. The reason to select this actuator is its surprising ability to produce different flow regimes only by changing the actuation parameters, i.e. frequency and amplitude without changing the geometrical parameters.

The current JaVA system evolved from an earlier flow actuator developed by Jacobson and Reynolds (1998) which consists of a cantilevered beam oscillating in a cavity and which was tested in water. However, the active flow control actuator (JaVA) of the present study consists of a cavity and a rigid plate that is placed at the top of the cavity such that it forms a narrow and a wide gap when viewed from the top, see Fig. 1. The plate is oscillated in the vertical direction such that the plate motion is uniform along its length and

* Corresponding author. Tel.: +49 711 6856 3401; fax: +49 711 6856 3438.
E-mail addresses: rashad@iag.uni-stuttgart.de (M.A. Rashad), rist@iag.uni-stuttgart.de (U. Rist).

Nomenclature

f	actuator plate vibration frequency	t	time
a	actuator plate amplitude (mean to peak plate distance)	$T = 1/f$	oscillation period
$S_a = 2\pi a/b$	scaled amplitude	U_p	plate velocity
w_n	narrow gap width	$\mathrm{Re} = U_p b/\nu$	Reynolds number
w_w	wide gap width	U, u	velocity
b	plate width	U_c	cross-flow velocity
$D = w_w + b + w_n$	actuator width	δ	boundary layer thickness
n-D	downstream distance from actuator end in diameters	Θ	oscillation phase angle w.r.t. actuator motion
$\omega = 2\pi f$	circular frequency		$y(t) = a\sin(\omega t)$
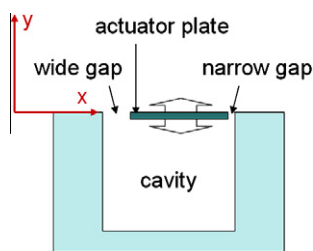
Fig. 1. Basic setup of the JaVA by Lachowicz et al. (1999a).

width. Thus, the actuator plate acts like a piston pumping air out of the cavity on the downstroke and sucking air into the cavity on its upstroke. This kind of active flow-control actuator produces different flow fields depending on the actuation parameters frequency and amplitude of the oscillating actuator plate: A free jet that emanates either from the narrow or the wide gap at controlled angles to the actuator surface, including a wall-parallel wall jet, and eventually a flow field with a large vortex above the plate, the so-called vortex mode of operation, cf. Lachowicz et al. (1999a) In Rashad and Rist (2010) we have simulated and confirmed these different actuation modes but for the present paper only the vortex mode of this actuator will be considered because this mode is the best documented in all previous investigations of the JaVA.

So far, there are only a few published attempts which tried to simulate the JaVA in a computational study. Joslin et al. (1998) and Lachowicz et al. (1999b) have modeled the mechanical parts of the JaVA actuator by unsteady velocity boundary conditions on a flat plate and obtained reasonable agreement with the vortex mode of the actuator observed in the experiments. Koumoutsakos (1995) has used a particle (vortex) method in Lagrangian frame to provide a qualitative explanation why the JaVA-induced flow field changes from jet to vortex type when the magnitude of oscillation through the gaps gets larger. He concludes that further research is necessary. As the vortex mode is the most documented in all previous investigations of the JaVA, we have chosen this mode of operation for comparison with Lachowicz et al. and also for our present investigations of its performance in a generic cross flow.

2. Numerical approach

The first step in any CFD simulation is to select an appropriate code according to the problem for the calculation of the flow field. For the present actuator-geometry simulations, use of the general purpose CFD software Fluent seemed to be the most appropriate, because of the need for simulating rather complex geometries with moving boundaries at different velocities. The accompanying grid-generation software GAMBIT is used for geometry specification and grid generation. The Fluent software appears to be well-suited and

established in the car industry for simulations of reciprocating engines because of its versatility to deal with dynamic meshes. Some recent examples for the use of Fluent for jet-actuator simulations can be found in Pinzon et al. (2008) and Zhou and Zhong (2008), for instance.

A structured, deformable dynamical grid with the option of sliding interfaces between different grid blocks is used in our case. This technique has advantages as there is no grid degeneration near the area of interest and also it is more robust compared to other alternatives. In order to move the grid and to apply boundary conditions at the plate and also for the inlet velocity boundary for the cases with cross-flow a special feature of Fluent called "user-defined functions (UDF)" is used.

The motion of the plate and grid is prescribed by the following set of equations

$$
\begin{aligned}
\omega &= 2\pi f, \\
y(t) &= a\sin(\omega t), \\
U_p(t) &= a\omega\cos(\omega t), \\
T &= 1/f,
\end{aligned}
\tag{1}
$$

where ω and f are the circular and the actuator-plate frequency, respectively. $y(t)$ denotes the instantaneous position of the actuator plate, a the oscillation amplitude, $U_p = dy/dt$ the instantaneous velocity of the actuator plate, and T the oscillation period.

Since only two-dimensional measurements are available from Lachowicz et al. (1999a) and the flow field in the middle of the actuator is considered to be two-dimensional (if placed in still air, i.e. without a free stream flow in the plane-normal direction), only two-dimensional simulations are carried out in the present study for comparison.

3. Grid and boundary conditions

Fig. 2 shows the setup and the integration domain used, together with its discretization into nine grid blocks for the case without cross flow. The number of grid cells in x and y direction of each block is given in the table in the insert and the boundary conditions are indicated using colors. Red[1] for the "free-stream" boundaries, where constant pressure is applied, it is therefore denoted as "pressure outlet", black for the "no-slip boundary condition" of the rigid cavity walls, denoted "cavity", and blue for the oscillating plate. Block numbers 1, 5, 6 and 8 are attached to the plate, i.e. they move up and down together with it while block numbers 2, 3, 4, 7 and 9 remain stationary throughout the simulation. The connections between rigid parts and the moving part of the domain are performed by so-called "sliding interfaces" (green lines), i.e. between blocks number 4 and 5 on the left side of the

---

[1] For interpretation of color in Figs. 1–12, the reader is referred to the web version of this article.
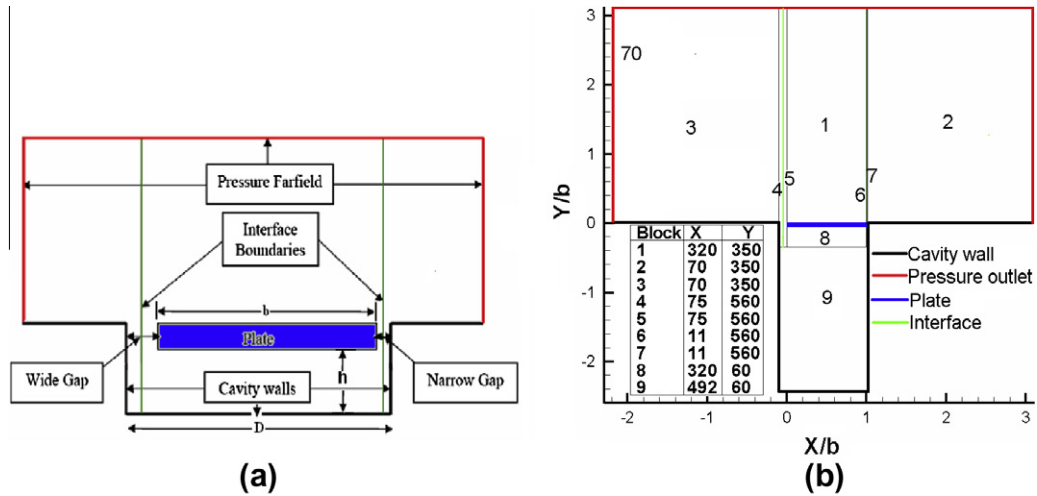
Fig. 2. Overview on geometry and boundary conditions (a) and grid block numbering with number of grid points per block (b).

actuator plate and between blocks number 6 and 7 on the right-hand side. When the plate moves up and down, the two adjacent grids slide at these interface boundaries with respect to each other. When the plate moves upward grid cells are eliminated at the top of block number 1 while at the same time grid cells are generated at the bottom of block number 8 and vice a versa, depending upon the remeshing parameters specified. Therefore, these boundaries are kept away from the area of interest. Block number 9 in this set-up is optional which means that, depending upon the required cavity depth; its vertical height can be varied or even completely removed for smaller cavity depths. For cases with cross-flow the domain after the actuator (to the right of it) is increased 10 times and also the pressure-far-field boundary conditions at the left and top of the domain are changed to velocity inlet.

4. Results

Many cases presented in Lachowicz et al. (1999a) have been simulated and compared with the available literature and it turned out that the present two-dimensional simulations capture the different jet-and-vortex flow regimes described by Lachowicz et al. very well, see Rashad and Rist (2010) and Fig. 3.

In the present paper three different cases will be presented. In the first case, results of Lachowicz et al. are reproduced numerically for the vortex mode of the actuator. This is done by performing simulations without cross-flow (i.e. in still air). In the second and third case simulations are performed with cross-flow by using the same flow parameters but different arrangements of the wide and narrow gaps with respect to the cross flow. In case-2 (configuration-1) the wide gap is on the left side (i.e. the upstream side of the cavity) while the narrow gap is on the other (downstream) side. In case-3 (configuration-2) the gap orientation is reversed (i.e. narrow gap towards left and wide gap towards right) while the flow direction is still the same (positive x-direction). The domain after the actuator in each case is increased to 10D in order to see the effects on the flow for a longer distance. All simulations are performed for laminar flow without any turbulence model because of the low Reynolds numbers encountered in the according laboratory experiments by Lachowicz et al. (1999a) ($Re_{plate} = U_p b / \nu = 149$), where b is the actuator-plate width. For the cases with cross flow we have chosen $Re_\delta = U_c \delta / \nu = 667$ as the boundary-layer Reynolds number. The inflow velocity profile is computed from $u(y/b) = U\_c * \tanh(2.564\, y/b)$.
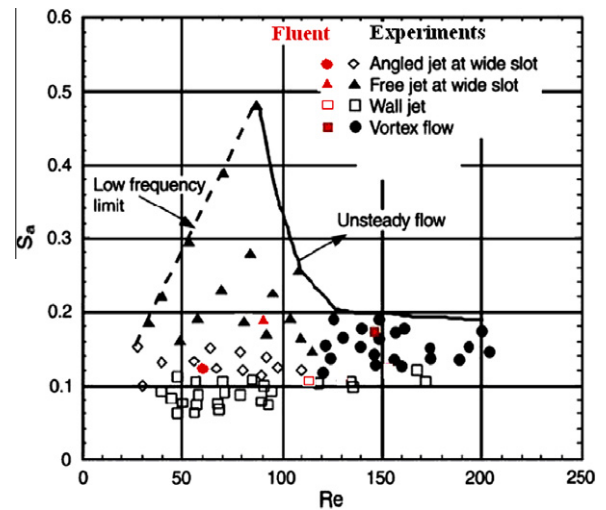
Fig. 3. Comparison of simulated flow regimes with experiments by Lachowicz et al.; Re = Reynolds number, Sa = scaled amplitude.

4.1. Case 1

The simulations are performed at frequency $f = 128$ Hz and scaled amplitude $S_a = 2\pi a/b = 0.1829$ for air at room conditions. The maximum plate velocity $U_{p,\max} = 2\pi a f$ and plate length b are used to normalize all the velocities and lengths, respectively. The simulation has been run over 24 oscillation cycles T and the results are averaged over the last four cycles for comparison with Lachowicz et al. In Fig. 4 instantaneous results of the last cycle are shown. The relation between actuator-plate motion and the indicated non-dimensional time is as follows. The phase angle $\Theta = 0°$ corresponds to $t = 0$ in Eq. (1), where the actuator plate passes the mean position $y = 0$ on the upstroke. At quarter cycle ($\Theta = 90°$ e.g. $t = 23.25T$) the plate is at its upper turning point, at half cycle ($\Theta = 180°$ e.g. $t = 23.5T$) it passes the mean position at maximal downward speed, then at three-quarter cycle ($\Theta = 270°$, $t = 23.75T$) it turns at its lower turning point, and at the full cycle ($\Theta = 0°$ or $\Theta = 360°$) it passes the mean position at maximal upward speed. This means that the flow through the gaps is maximal at half and full cycle, because the plate periodically displaces fluid between inside and outside of the cavity. This effect can be seen in the contours of Fig. 4b and d as a red dot in the wide
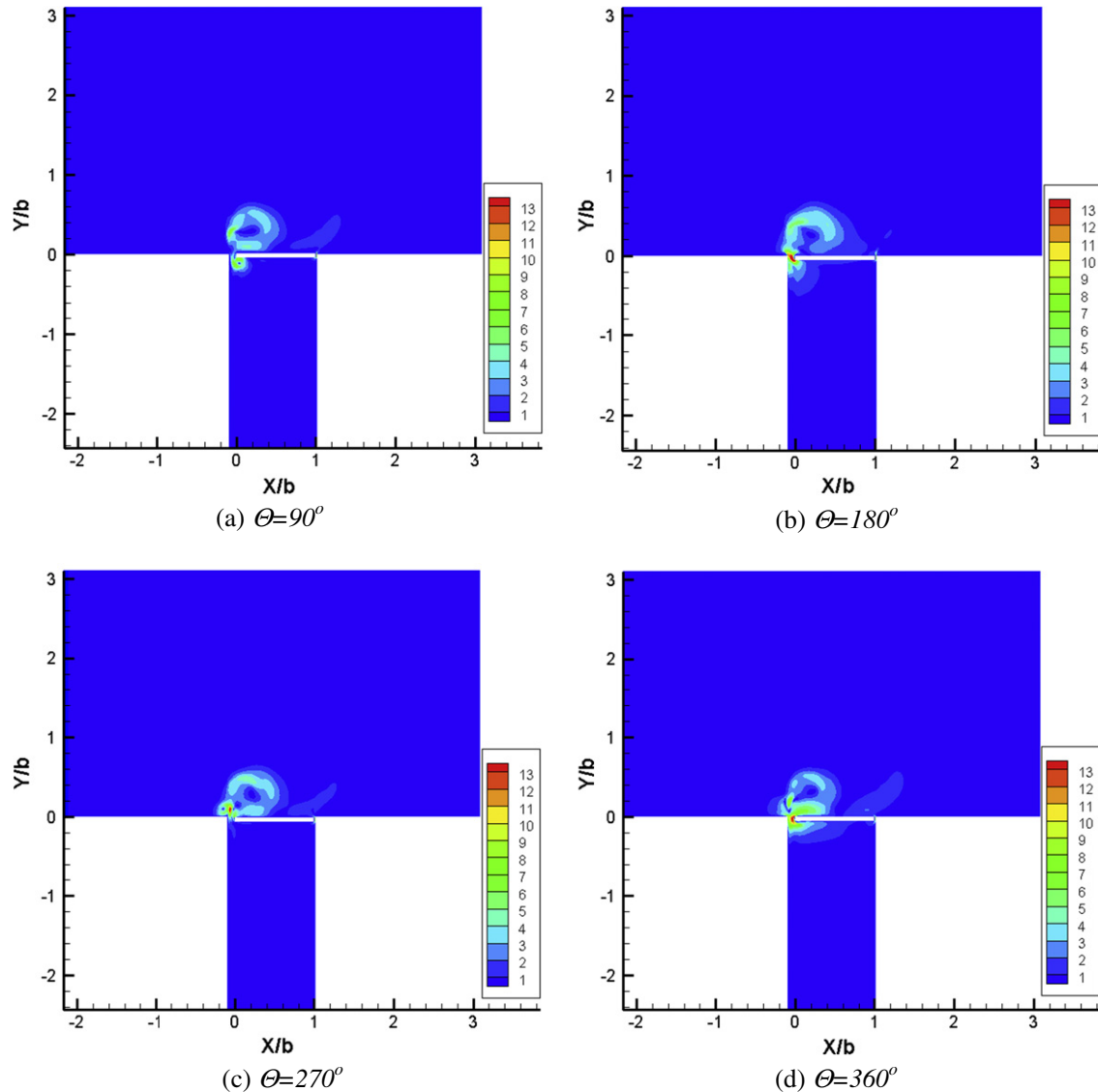
Fig. 4. Contours of instantaneous velocity magnitude at four different phases from the 24th oscillation cycle.

gap. The surprising feature of the JaVA in vortex mode is that the high-speed fluid ejected from the cavity at the wide-gap side rolls up into a vortex above the plate. A smaller vortex appears inside the cavity during the suction phase.

Major fluid motions induced by the oscillating plate are confined to the area surrounding the plate, as expected. However, compared to the maximum velocity of the actuator, a much larger velocity occurs in the wide gap in order to maintain continuity. As the oscillator moves up and down it accelerates the fluid in the gap and pushes it downward or sucks it upwards. During each actuator cycle a pulse of high-speed fluid ejects from the wide gap. Each of these velocity pulses is a sign of a counter-rotating vortex pair that gets ejected from the wide gap at each cycle. With increasing distance from the orifice these pulses merge with the average flow field induced by the previous cycles, thus strengthening the outside vortex.

The time averaged velocity field resulting from the instantaneous events shown in Fig. 4 is illustrated in Fig. 5a. The outer flow field is dominated by the big vortex above the actuator plate, part of a start-up vortex which disappears after much longer simulation time appears above the right gap, and a small vortex is present inside the cavity below the wide gap. Grid refinements have shown

that the size of the outer vortex is mesh dependent. So, special care was required to get a mesh-independent solution. Other parameters which affect the outer flow field are the plate position with respect to the cavity top wall and the cavity depth.

The other parts of Fig. 5 shows the time averaged results of Joslin et al. (1998) in subfigure (b) and a LIC visualization, see Cabral and Leedom (1993), of the present results in subfigure (c) for comparison with the visualizations of Lachowicz et al. (1999a) in subfigure (d). The qualitative comparison of our own results in subfigures (a) and (c) with the stream lines provided by Lachowicz et al. (1999a) and Joslin et al. (1998) in subfigures (b) and (d) turns out to be excellent. Comparing the size of the vortex with respect to the width of the actuator it appears that the size of the vortex in our case is almost the same as the one observed in the experiments by Lachowicz et al.

Computational and experimental time-averaged velocity profiles along a vertical cut through the vortex center are quantitatively compared in Fig. 6a. This comparison once again shows that the vortex size in our case is almost the same as the one observed by Lachowicz et al. (1999a) in their experiments. The positive and negative velocity magnitude maxima agree with the experimental results better than the results of the numerical
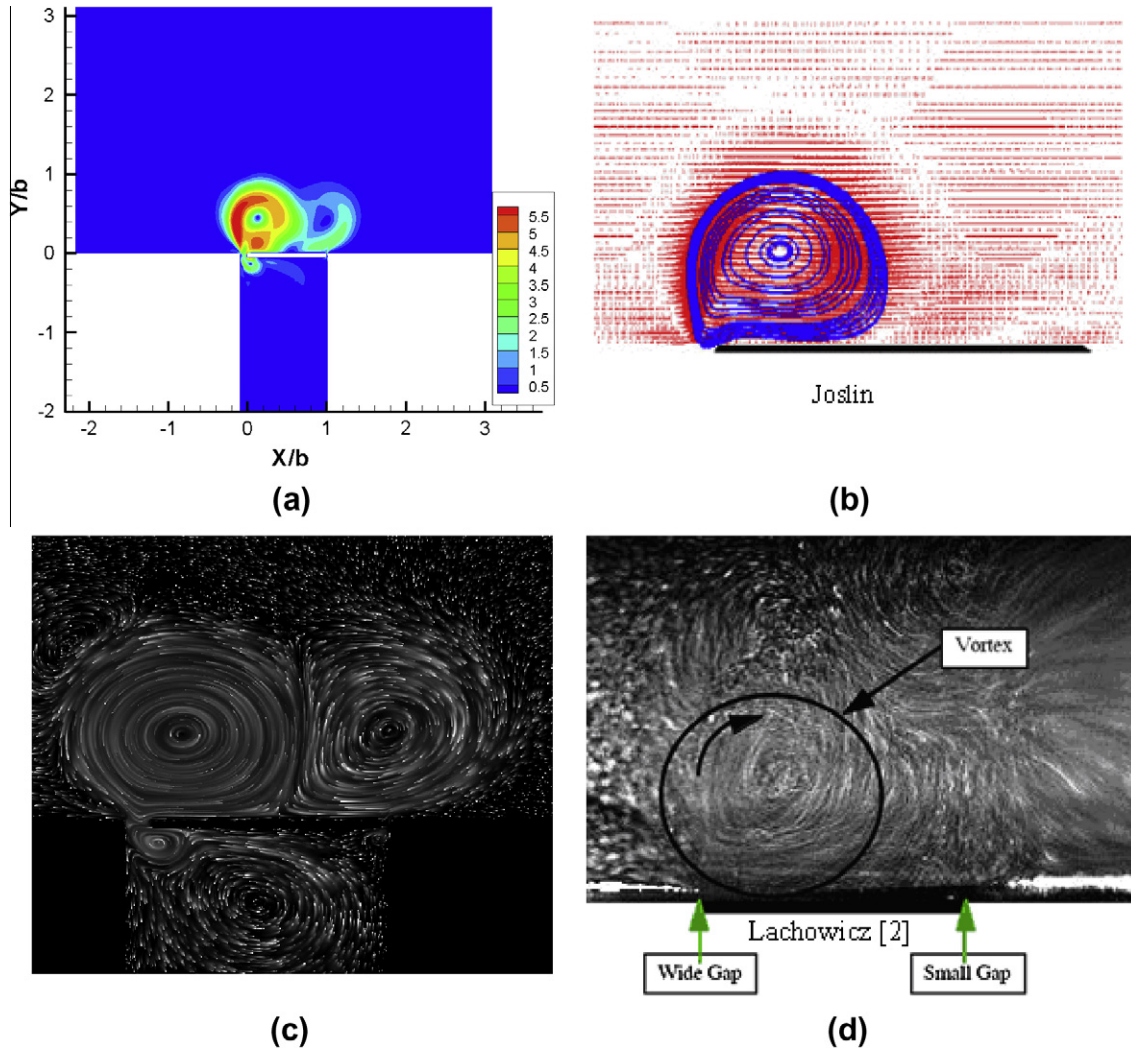
Fig. 5. Comparison of averaged velocity fields. (a) and (c) present results, (b) Joslin et al. (1998), and (d) Lachowicz et al. (1999a). Note that subfigure (c) shows CFD data using LIC according to Cabral and Leedom (1993) which makes it look like a real photo.

modeling performed by Joslin et al. (1998). Fig. 6b shows the plots of instantaneous velocity in the wide gap for eight different phases of the oscillation. It can be seen that the flow is very complex containing flow separation and reverse flow. We can observe that the velocity is not evenly distributed inside the gap and also blowing is stronger than suction. During the blowing phase the high-speed fluid is closer to the cavity wall while during the suction phase high-speed fluid is closer to the moving plate. Looking more closely at this figure we can also see that near the plate the flow is opposite to the main flow which is more significant during blowing. The reason for this complex flow behavior is that the wide gap width is very large compared to the plate thickness. We now turn to the narrow gap. Fig. 6c, shows the plots of instantaneous velocity in the narrow gap for eight different phases of oscillation. Here, the flow is more like a mixed Couette–Poiseuille flow simply because the narrow gap width is very small compared to the plate thickness. Another typical observation (for oscillating viscous flows) is that the velocity profiles are not symmetric during outward and inward flow. In addition, the maximal outflow velocity does not occur in phase with the plate oscillation. It occurs about 45° after the plate has reached its upper or lower turning point ($\theta = 90°$ or $\theta = 270°$). There is no such phase shift in the wide gap.

In Table 1 flow rates through the gaps are compared with the fluid that is pushed by the plate at eight different time instances

during the 24th period of oscillation. To make sure that the use of a dynamical grid with sliding mesh interfaces does not have a negative impact on the conservation of mass, we compared the plate- and gap-net-flow rates given here. It turned out that mass is conserved with an error smaller than 2.1% at every time instance in the present computations. As already observed above, there is a phase shift in the narrow gap with respect to the plate motion which is typical for harmonically oscillating flows, like the so-called second Stokes' problem which can be observed here as well. The maximum flow through the narrow gap occurs at $\theta = 135°$ and $\theta = 315°$ in contrast to the maximum of fluid displaced by the plate which occurs at $\theta = 360°$ and $\theta = 180°$, respectively. Since the wide gap is much wider there is no such phase shift there. The net flow through the wide gap is the strongest and thus drives the flow outside the cavity. At $\theta = 90°$ and $\theta = 270°$ where the plate is at rest (which means zero flow rate), there is still some flow through the gaps (especially in the narrow gap) because of the above phase shift. Also in the wide gap the flow is not zero because the fluid close to the plate still follows the previous motion of the plate due to its inertia in spite of the plate being at rest again. The according in- or outflow near the plate is not fully compensated by an according out- or inflow in the other (left) part of the wide gap and the instantaneous net flow rate through the wide gap is also not zero at these phase angles.
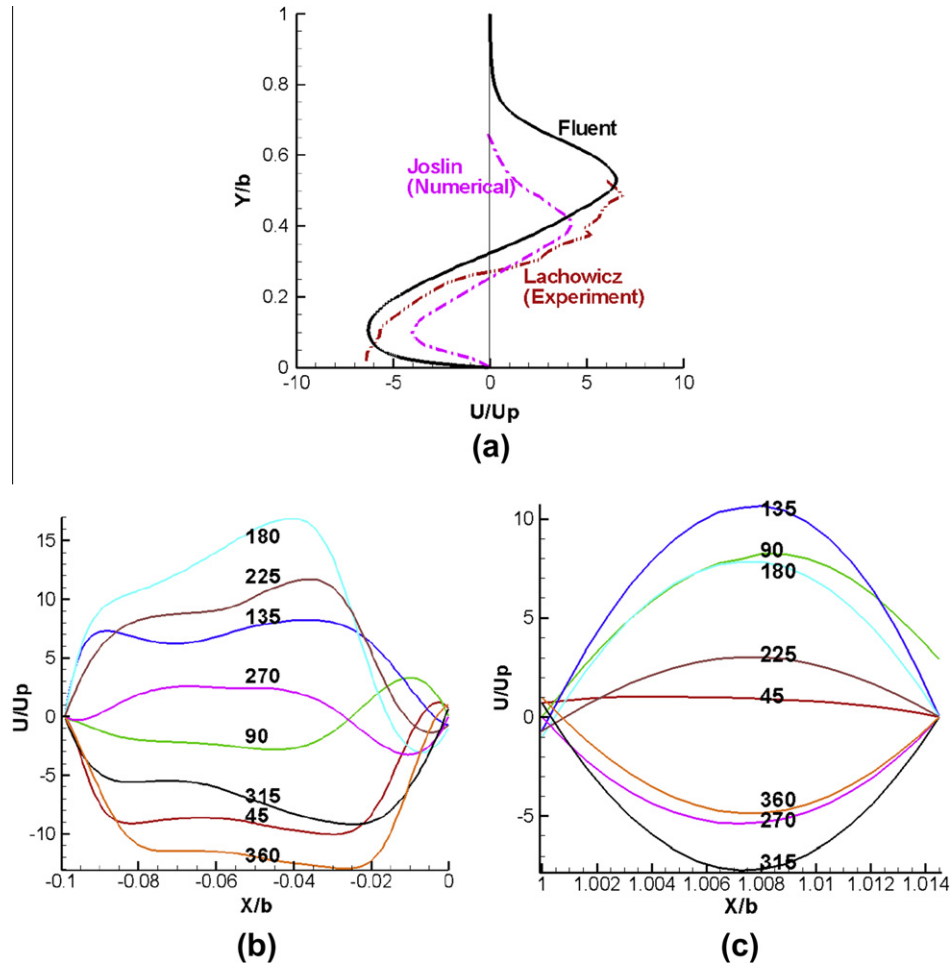
Fig. 6. Comparison of velocity profiles: (a) mean velocity profiles in a vertical cut through the vortex center, (b) and (c) instantaneous velocities in a horizontal cut through the wide and narrow gap, respectively.

Table 1
Comparison of volume flow rates at different phases of the actuator cycle.

Phase (°)	Plate m³/s (10^{-3})	Narrow gap m³/s (10^{-3})	Wide gap m³/s (10^{-3})
45	1.522	0.0307	−1.585
90	0	0.1906	−0.2077
135	−1.522	0.20614	1.323
180	−2.181	0.1460	2.038
225	−1.522	0.0377	1.516
270	0	−0.1205	0.1402
315	1.522	−0.1549	−1.373
360	2.181	−0.0961	−2.085

4.2. Case 2: configuration-1

In this case the simulation is performed at a frequency of 128 Hz and scaled amplitude of 0.1829, i.e., the same as in case 1, but now with a cross flow velocity of $U_c/U_p = 4.425$. This simulation is run for thirty oscillation periods and averaged over the last ten periods. Results presented here are for the last oscillation period.

In Fig. 7 contours of mean velocity magnitude are shown. They indicate a large counter-clockwise turning vortex in the left part of the cavity, a very large separation bubble above the actuator plate and an area of high-speed fluid in the free stream above the actuator. The boundary layer downstream of the actuator seems slightly thinner. The zoom-in-view in subfigure (b) above the plate shows details of the big elongated separation bubble which covers the whole plate and extends further to 0.5b to the right of the narrow gap. The height of the bubble is almost half the boundary layer thickness δ. The bubble is driven by the fluid ejected from the wide gap. Especially at the wide gap there is a net upward flow in the mean above the left part of the gap, which explains the occurrence of the large separation bubble, because this jet displaces the oncoming boundary layer away from the wall. Compared to the case without cross flow the narrow gap is now also somewhat more active. After the bubble the flow is re-directed towards the wall where it reattaches and produces fuller boundary layer velocity profiles as can be seen in Fig. 8 which shows velocity profiles at different distances from the actuator for comparison with the cross-flow reference profile used at inflow (left part of the figure).
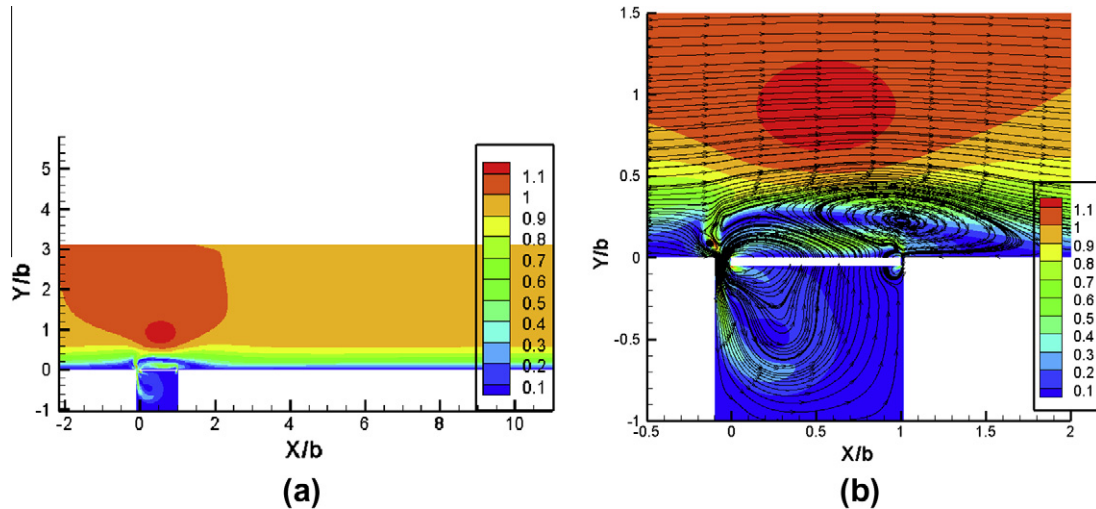
Fig. 7. Contours of mean velocity magnitude normalized with respect to cross-flow velocity U_c, configuration-1.
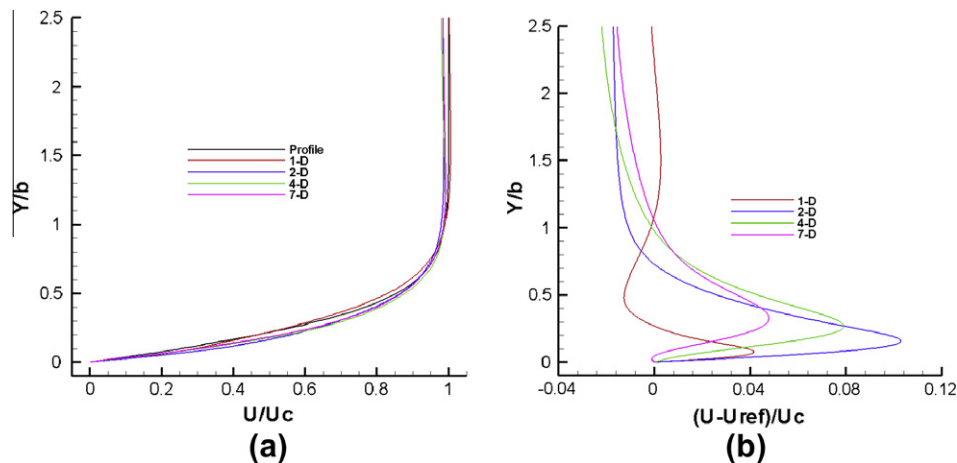
Fig. 8. Mean velocity profiles at different *x*-distances, configuration-1.

For a better perception of the differences to the reference profile the difference $(U - U_{ref})/U_c$ is plotted in the right part of the figure. Here "reference profile" stands for the profile at the same distance from the inflow but for the unactuated flow. The distance from the actuator is given with respect to the length scale $D = 1.1135b$, which is the actuator width, i.e. the sum of plate width and narrow and wide gap widths. The inflow boundary-layer thickness used for the simulations is $1.063b$. Thus, actuator width D and boundary layer thickness δ are almost the same in the present work.

At a distance of 1-D after the actuator we see that the profile close to the wall (red line) is almost on top of the reference profile (black line) until a vertical distance of $0.28b$, after which it decreases faster. At the edge of the boundary layer there is a small overshoot, as already mentioned in the contour plots above (red area in Fig. 7). The close-up in subfigure (b) confirms that the red profile merely oscillates around the reference. Further downstream, at distances 2-D, 4-D, and 7-D all profiles are all almost the same. Compared to the reference they show the opposite effect compared to the first profile, i.e., that the velocity inside the boundary layer is higher now while it is smaller outside the boundary layer. Such an increase of speed close to the wall is what we wanted to achieve with the actuator. It would help to delay flow separation from the wall if the boundary-layer flow encountered

a region of adverse pressure gradient further downstream. The quantitative magnitude of this effect can be judged from Fig. 8b. It has a maximum of about 10% at 2-D distance and the decreases to 4% at 7-D.

4.3. Case 3: configuration-2

In this case the gap orientation with respect to the cross flow is inverted now with respect to the previous case, see Fig. 9. All other simulation parameters and the post processing are the same as before.

The contours of mean velocity magnitude in Fig. 9 shows a big vortex inside the right part of the cavity, a small separation zone on the left side of the plate, and a downstream boundary layer that is thicker than before and has a higher wall-friction at the same time. The cavity vortex is again fed by the wide gap but it turns in clockwise direction in the present case, because the arrangement of the gaps with respect to the plate has been reversed. This causes a significant suction above the gap which re-attaches the boundary layer! This time there is also no overshoot of the freestream velocity above the actuator.

The effects on the boundary layer velocity profiles are shown in Fig. 10 in the same way as before. Looking at the first profile (red
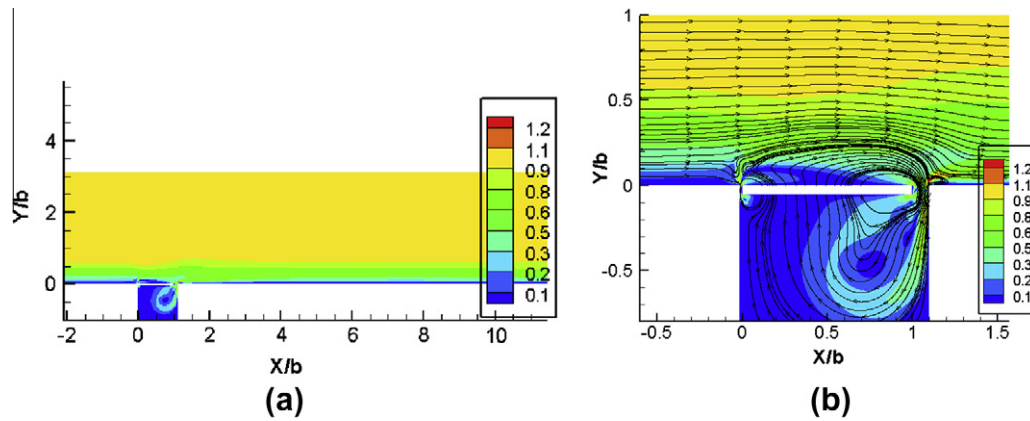
Fig. 9. Contours of mean velocity magnitude normalized with respect to cross-flow velocity U_c, configuration-2.
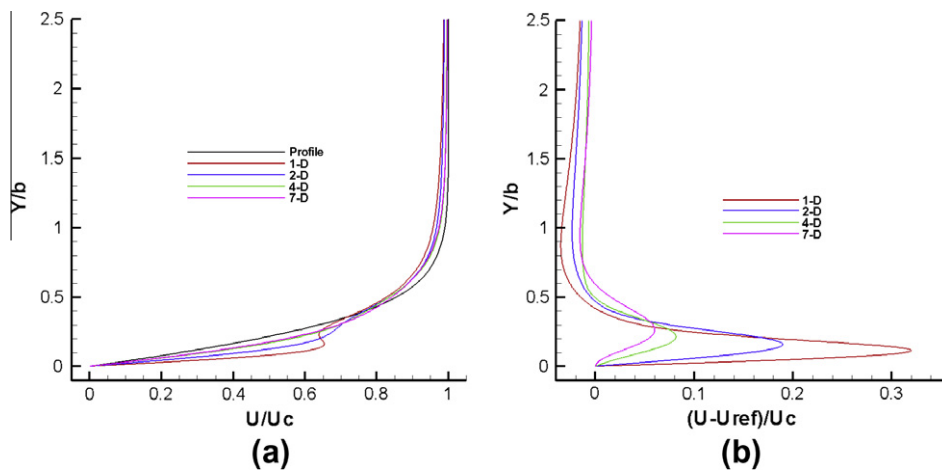
Fig. 10. Mean velocity profiles at different x-distances, configuration-2.

(a) narrow gap   (b) wide gap
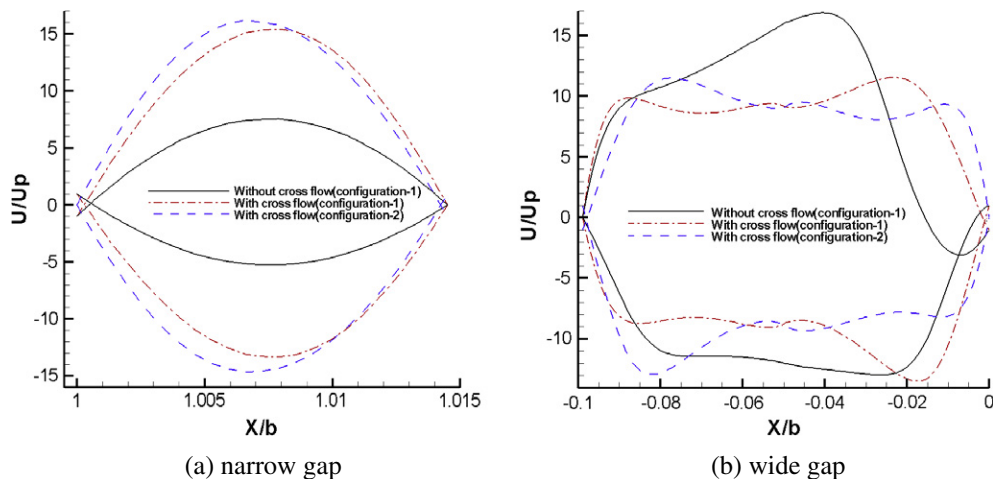
Fig. 11. Comparison of velocity profiles in narrow and wide gap.

line) at a distance of 1-D after the actuator, the boundary layer is now immediately much more attached to the wall compared to the original profile (black line). The velocity is higher inside the boundary layer until a vertical distance of about $0.4b$ after which it jumps back to the value of the reference profile. From then on the velocity stays below the reference. Now, the maximal over-shoot close to the wall is about 20% of the free-stream velocity compared to only 10% in the previous case (compare Figs. 8b to 10b) at a distance 2-D. The first profile looks as if a small vortex were overlaid on the boundary layer. A similar behavior can be observed with the next profile at 2-D distance (blue line) but with smaller effects. The other profiles at a distance of 4-D and 7-D

(a) x=1-D

(b) x=2-D
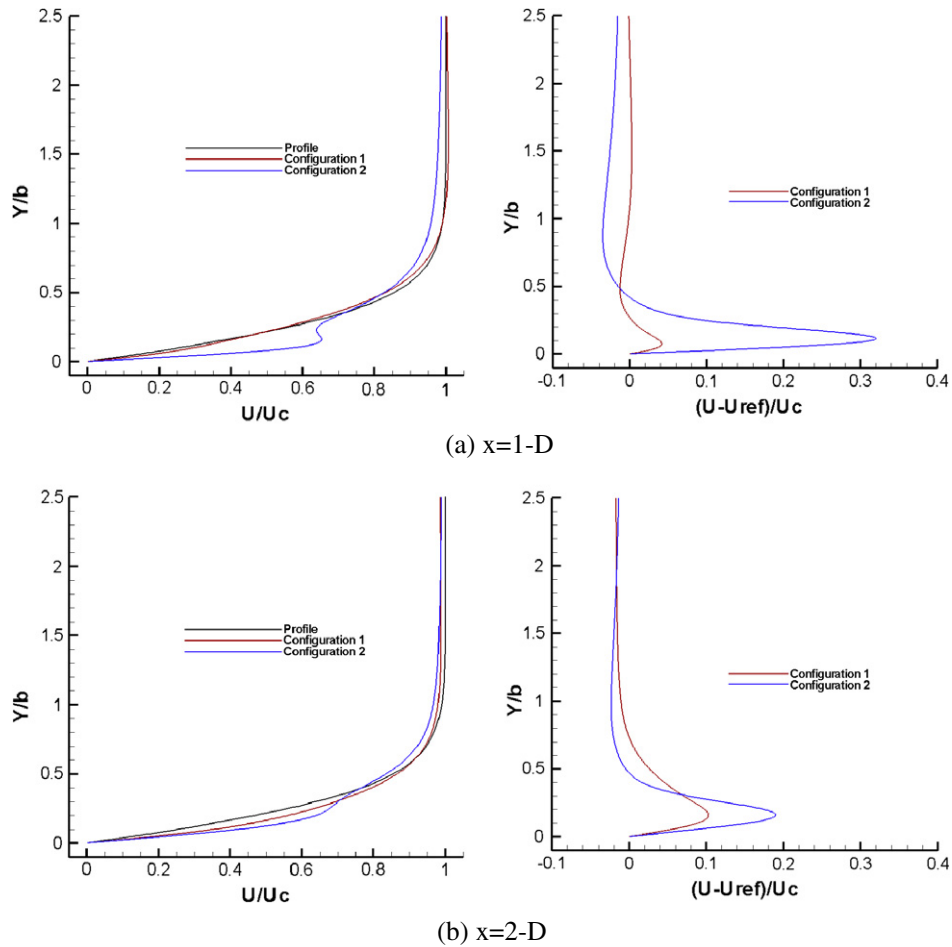
Fig. 12. Comparison of velocity profiles at different *x*-positions.

are largely undisturbed but inside the boundary layer a slightly higher velocity and outside the boundary layer a slightly lower velocity still occur. Their difference to the reference flow is still between 6% and 8%, i.e. larger than in the previous case discussed above.

4.4. Comparison

In Fig. 11a and b velocity profiles in the narrow and wide gap respectively are compared for all three cases at two time instances, when the plate is at maximum velocity. In the narrow gap both suction and blowing velocities for the cases with cross flow are very high compared to the case without cross flow. Peak velocities are almost twice as large. When we compare the profiles in the wide gap there are two velocity peaks in the cases with cross flow while in the case without it there is only one peak during blowing and the profile is flat during suction. Note that in the cases with cross-flow, there is no reverse flow near the plate in contrast to the case without cross-flow, where there is a strong reverse flow near the plate. These comparisons show that the flow through the gaps 'communicates' with the cross flow.

Fig. 12 shows the comparison of boundary-layer velocity profiles at different positions after the actuator for the cases with cross-flow. It can be seen that in configuration-1 (red lines) there is no significant difference from the original profile in obvious contrast to configuration-2 where a strong effect of actuation can be seen until the distance $x = 2$-D. The boundary layer profiles of configuration-2 (blue lines) are more attached to the wall compared to the original profile (black line) until a vertical distance

of $0.5b$, and the velocity is very high until this distance. Afterwards there is a jump and the velocity decreases relative to the original profile. The effect at a distance of 2-D is the same but to a lesser extent.

5. Conclusions

The Jet and Vortex Actuator (JaVA) originally presented by Lachowicz et al. (1999a) was characterized in still air and also with cross flow using flow visualization and mean velocity measurements. Three different cases were studied. In the first case simulations were performed in still air to reproduce the experimental results of Lachowicz et al. (1999a) in the computer simulations by using the commercial CFD software Fluent®. It was found that the simulation results are in an excellent agreement with the literature.

In the last two cases simulations were performed with cross-flow using opposite arrangements of the wide and narrow gaps with respect to the cross flow. In the first case, where the wide gap is placed at the upstream end of the actuator, a large separation bubble develops above the actuator which first displaces the boundary-layer flow away from the wall. After re-attachment the boundary-layer profiles are slightly fuller than before such that the wall friction increases which is good for separation control. Reversing the actuator arrangement by placing the narrow gap at the upstream end makes the same actuator even more efficient. The near-wall velocity difference with respect to the unactuated flow increases by a factor of two compared to the first case. This is caused by a much smaller separation bubble above the actuator

plate and mean-flow suction provided by the wide gap at the downstream end of the actuator which helps to actively re-attach the boundary layer. Overall, both present configurations are capable of increasing the near-wall fluid momentum in the boundary layer downstream of the actuator which would be a good prerequisite for separation delay. At present we do not claim to have found the optimum configuration because the effects of actuation amplitude and frequency as well as the influence of the actuator plate's mean position are not treated here. Such additional details are treated in a similar study by Cadirci et al. (2010).

In summary it can be said that the JaVA can be used to re-energize a boundary layer flow close to the wall which is a necessary condition for separation delay, like many other zero-net mass flux devices investigated before. It can also be said that the orientation of the gaps of such a device with respect to the flow direction has an influence. However, it cannot be said yet whether the JaVA works better or worse than other devices. This question needs extra work.

References

Cabral, B., Leedom, L.C., 1993. Imaging vector fields using line integral convolution. In: SIGGRAPH 1993 Conference Proceedings, pp. 263–270.

Cadirci, S., Gunes, H., Rist, U., 2010. Numerical Investigation of Jet and Vortex Actuator (JaVA) for active flow control. AIAA paper 2010-4410. In: 5th Flow Control Conference, Chicago, IL, 28 June–1 July.

Gad-el-Hak, M., 2000. Flow Control, Passive, Active, and Reactive Flow Management. Cambridge University Press.

Gad-el-Hak, M., 2001. Flow control: the future. Journal of Aircraft 38, 402–418.

Gad-el-Hak, M., Bushnell, D.M., 1991. Separation control: review. Journal of Fluids Engineering 113 (March), 5–33.

Glezer, A., Amitay, M., 2002. Synthetic jets. Annual Review of Fluid Mechanics 34, 503–529.

Godard, G., Foucaut, J., Stanislas, M., 2006. Control of a decelerating boundary layer. Part 2: optimization of slotted jets vortex generators. Aerospace Science and Technology 10, 394–400.

Jacobson, S.C., Reynolds, W.C., 1998. Active control of stream wise vortices and streaks in boundary layers. Journal of Fluid Mechanics 360, 179–994.

Joslin, R.D., Lachowicz, J.T., Yao, C., 1998. DNS of flow induced by a multi-flow actuator. ASME paper Number FEDSM98-5302, ASME Fluid Engineering Meeting.

Koumoutsakos, P., 1995. Simulations of vortex generators, center for turbulence research. Annual Research Briefs, 233–240.

Lachowicz, J.T., Yao, C., 1998a. Flow field characterization of a jet and vortex actuator. Experiments in Fluids 27, 12–20.

Lachowicz, J.T., Yao, C.-S., Joslin, R.D., 1999b. Physical analysis and scaling of a jet and vortex actuator. FEDSM99-6921, 3rd ASME/JSME Joint Fluids Engineering Conference, July 18–22, San Francisco, Ca.

Lin, J.C., 2002. Review of research on low-profile vortex generators to control boundary-layer separation. Progress in Aerospace Sciences 38, 389–420.

Lockerby, D.A., Carpenter, P.W., 2004. Modeling and design of microjet actuators. AIAA Journal 42, 220–227.

Pinzon, C., Agarwal, R., Wright, P., 2008. Effect of compressibility in modeling of a zero-net-mass-flux actuator: an experimental and computational study. AIAA-2008-3764. In: 4th Flow Control Conference, Seattle, Washington, June 23–26.

Rashad, M.A., Rist, U., 2010. Numerical investigation of a Jet and Vortex Actuator (JaVA). In: Dillmann, A., Heller, G., Klaas, M., Kreplin, H.P., Nitsche, W., Schröder, W. (Eds.), Notes on Numerical Fluid Mechanics and Multidisciplinary Design 112, New Results in Numerical and Experimental Fluid Dynamics VII. Contributions to the 16. STAB/DGLR-Symposium Aachen, Germany 2008. Springer, pp. 217–224.

Tang, H., Zhong, S., Jabbal, M., Garcillan, L., Guo, F., Wood, N., Warsop, C., 2007. Towards the design of synthetic-jet actuators for full-scale flight conditions Part 2: low-dimensional performance prediction models and actuator design method. Flow, Turbulence and Combustion 3-4, 309–329.

Zhong, S., Jabbal, M., Tang, H., Garcillan, L., Guo, F., Wood, N., Warsop, C., 2007. Towards the design of synthetic-jet actuators for full-scale flight conditions Part 1: the fluid mechanics of synthetic-jet actuators. Flow, Turbulence and Combustion 3-4, 283–307.

Zhou, J., Zhong, S., 2008. Numerical simulation of the interaction of a circular synthetic jet with a laminar boundary layer. AIAA-2008-3994. In: 4th Flow Control Conference, Seattle, Washington, June 23–26.